(e.g., PH33-3) and those with low (^{230}Th/^{238}U) < 1.0 (e.g., PH34-1) suggests spatially restricted magma transport routes to the surface for some off-axis volcanism. In addition, near-symmetrical off-axis eruptions in a broad region are more consistent with passive mantle flow driven by plate motion (*1*, *2*) than with active mantle flow driven by buoyancy in a narrow region (about a few kilometers).

References and Notes

1. D. W. Forsyth *et al*., *Science* **280**, 1215 (1998).
2. M. Spiegelman, J. R. Reynolds, *Nature* **402**, 282 (1999).
3. J. R. Reynolds, C. H. Langmuir, *G*^{3} **1**, 1999GC000033 (2000).
4. S. J. Goldstein, M. R. Perfit, R. Batiza, D. J. Fornari, M. T. Murrell, *Nature* **367**, 157 (1994).
5. P. Gente, J. M. Auzende, V. Renard, Y. Fouquet, D. Bidean, *Earth Planet. Sci. Lett.* **78**, 224 (1986).
6. S. Carbotte, K. Macdonald, *J. Geophys. Res.* **97**, 6959 (1992).
7. Glass chips (<500 μm) were carefully picked under a binocular microscope to avoid oxides or alteration coatings, ultrasonically cleaned, and then ground by hand in an agate mortar. Picked glass was then leached in a 1:1 mixture of 30% H_2O_2 and 2.5 M HCl for 10 min at room temperature to efficiently dissolve and remove Mn oxides without affecting Th/U ratios. Samples for U-Th isotope analyses were spiked with a ^{233}U-^{229}Th spike and dissolved in a HF-$HClO_4$–HCl-HNO_3 mix, and samples for Pb isotope analyses were dissolved in a HF-HBr mix. Th isotopes were measured by ISOLAB 54, and U and Pb isotopes were measured by MAT 262 RPQII. Chemically purified Th was loaded with colloidal graphite onto a pyrolitically coated graphite rod and ionized with a primary Ar^+ ion beam. This technique yields high Th ionization efficiencies (0.5 to 2%). Repeat analyses of a Th standard solution WUN-1 yielded a mean of $4.297 \pm 0.045 \times 10^{-6}$ (2σ) for (^{230}Th/^{232}Th) atomic ratios. U, loaded with colloidal graphite, was ionized on a single Re filament, and the (^{235}U/^{238}U) ratio was used to correct for mass fractionation. Pb samples were loaded with concentrated silica gel onto single Re filaments. Pb isotope data were corrected for fractionation of 0.13% per atomic mass unit for ^{206}Pb/^{204}Pb, ^{207}Pb/^{204}Pb, and ^{208}Pb/^{204}Pb, based on repeated analyses of standard NBS-981. Measured values for the Pb NBS-981 standard were 36.507 ± 0.012 for ^{208}Pb/^{204}Pb, 15.430 ± 0.004 for ^{207}Pb/^{204}Pb, and 16.891 ± 0.003 for ^{206}Pb/^{204}Pb. Trace element concentrations were measured on cleaned glass chips with a PQ2 inductively coupled mass spectrometer. For more detailed descriptions of the trace element and isotope analytical methods, see (*32*–*34*).
8. D. McKenzie, *Earth Planet. Sci. Lett.* **72**, 149 (1985).
9. M. Spiegelman, T. Elliott, *Earth Planet. Sci. Lett.* **118**, 1 (1993).
10. C. C. Lundstrom, J. Gill, Q. Williams, M. R. Perfit, *Science* **270**, 1958 (1995).
11. H. Zou, A. Zindler, *Geochim. Cosmochim. Acta* **64**, 1809 (2000).
12. R. Batiza *et al*., *Geophys. Res. Lett.* **23**, 221 (1996).
13. Supplementary data on major and trace element concentrations are available on *Science* Online at www.sciencemag.org/cgi/content/full/295/5552/107/DC1.
14. S. J. Goldstein, M. T. Murrell, R. W. Williams, *Earth Planet. Sci. Lett.* **115**, 151 (1993).
15. B. Bourdon, A. Zindler, T. Elliott, C. H. Langmuir, *Nature* **384**, 231 (1996).
16. *D* depends on the mineralogy of the source rock and is given by
$$D = \sum_{1}^{n} x_i K_i$$
where x_i is the mass fraction of mineral *i* in the solid source, K_i is the mineral/melt partition coefficient of mineral *i*, and *n* is the total number of minerals.
17. P. Beattie, *Nature* **363**, 63 (1993).
18. M. M. Hirschmann, E. M. Stolper, *Contrib. Mineral. Petrol.* **124**, 185 (1996).
19. V. J. M. Salters, J. Longhi, *Earth Planet. Sci. Lett.* **166**, 15 (1999).
20. B. J. Wood, J. D. Blundy, J. A. C. Robinson, *Geochim. Cosmochim. Acta* **63**, 1613 (1999).
21. T. Z. LaTourrette, D. S. Burnett, *Earth Planet. Sci. Lett.* **110**, 227 (1992).
22. P. Beattie, *Earth Planet. Sci. Lett.* **117**, 379 (1993).
23. E. H. Hauri, T. P. Wagner, T. L. Grove, *Chem. Geol.* **117**, 149 (1994).
24. The LREE-enriched patterns in PH10-2 and PH34-1 may result from melting of a garnet peridotite source or an LREE-enriched spinel peridotite source. Their (^{230}Th/^{238}U) ratios of smaller than unity argue against the presence of garnet in the source. Low (^{230}Th/^{238}U) ratios of 0.85 to 0.90 can be modeled by dynamic partial melting of a spinel peridotite source when the porosity of the melting zone is 0.2%, the rate of melting is 1.0×10^{-4} kg m^{-3} year^{-1}, D_U = 0.0019, and D_{Th} = 0.0028 [see figure 2, A and D, in (*11*) for details].
25. R. A. Duncan, L. G. Hogan, *Geophys. Res. Lett.* **21**, 1927 (1994).
26. Y. Fialko, *Earth Planet. Sci. Lett.* **190**, 31 (2001).
27. The transport time for subsurface lateral movement (*t*) is given by the following relation:
$$t = -\frac{1}{\lambda_{230}} \ln \frac{(^{230}\mathrm{Th}/^{238}\mathrm{U}) - 1}{(^{230}\mathrm{Th}/^{238}\mathrm{U})_0 - 1}$$
where (^{230}Th/^{238}U) and (^{230}Th/^{238}U)$_0$ are the measured activity ratio in an off-axis sample and the activity ratio of the melt at the start of subsurface lateral transport, respectively. Dividing the distance from the axis (*d*) by *t* yields the average lateral velocity (*v*) of the melt that generated basalts PH8-1 and PH33-3: $v = d/t$. The lateral velocity of 19 to 21 cm year^{-1} is obtained by using (^{230}Th/^{238}U)$_0$ = 1.233. *v* increases when (^{230}Th/^{238}U)$_0$ decreases.
28. A. W. Hofmann, *Earth Planet. Sci. Lett.* **90**, 297 (1988).
29. S. S. Sun, W. F. McDonough, in *Magmatism in the Ocean Basins,* A. D. Saunders, M. J. Norry, Eds. (Geological Society Special Publication, London, 1989), vol. 42, pp. 313–345.
30. A. W. Hofmann, W. M. White, *Earth Planet. Sci. Lett.* **57**, 421 (1982).
31. B. L. Cousens, in *Earth Processes: Reading the Isotopic Code*, A. R. Basu, S. R. Hart, Eds. (American Geophysical Union, Washington, DC, 1996), vol. 95, pp. 207–231.
32. Y. Niu, R. Batiza, *Earth Planet. Sci. Lett.* **148**, 471 (1997).
33. J. G. England *et al*., *Int. J. Mass Spectrom. Ion Processes* **121**, 201 (1992).
34. B. Bourdon, thesis, Columbia University, New York (1994).
35. M. R. Perfit *et al*., *Geology* **22**, 375 (1994).

36. We thank R. Batiza for the samples; A. Sachi for chemistry; two referees for constructive reviews; and M. Reid, V. Salters, R. Odom, D. Loper, A. Stracke, and J. Simon for discussions and help. Supported by NSF grant EAR-9628083 (A.Z.) and NSF postdoctoral fellowship EAR-9805687 (H.Z.).

11 July 2001; accepted 13 November 2001

Formation of Recent Martian Debris Flows by Melting of Near-Surface Ground Ice at High Obliquity

F. Costard,[1] F. Forget,[2]* N. Mangold,[1] J. P. Peulvast[1]

The observation of small gullies associated with recent surface runoff on Mars has renewed the question of liquid water stability at the surface of Mars. The gullies could be formed by groundwater seepage from underground aquifers; however, observations of gullies originating from isolated peaks and dune crests question this scenario. We show that these landforms may result from the melting of water ice in the top few meters of the martian subsurface at high obliquity. Our conclusions are based on the analogy between the martian gullies and terrestrial debris flows observed in Greenland and numerical simulations that show that above-freezing temperatures can occur at high obliquities in the near surface of Mars, and that such temperatures are only predicted at latitudes and for slope orientations corresponding to where the gullies have been observed on Mars.

The observation of small gullies on Mars was one of the more unexpected discoveries of the Mars Observer Camera (MOC) aboard the Mars Global Surveyor spacecraft (*1*). The characteristics of these landforms suggest the local occurrence of a fluid emanating from alcoves located mostly in the upper part of poleward-facing slopes at mid- and high latitudes. Thick accumulations of debris cover the bases of escarpments, whereas the upper parts of the walls have generally steep slopes that are dissected by funnels (Fig. 1A). Malin and Edgett (*1*) convincingly argued that the gullies were probably created by debris flows composed of liquid H_2O mixed with rocks and residual water ice [alternative scenarios include speculations about liquid CO_2 breakout (*2*) and saline groundwater or brine (*3*)]. The lack of fresh impact craters and dust deposits suggest that the gullies are among

[1]UMR8616, Centre National de la Recherche Scientifique (CNRS), OrsayTerre, Équipe de Géomorphologie Planétaire, Université Paris-Sud, 91405, Orsay Cedex, France. [2]Laboratoire de Météorologie Dynamique, CNRS, Université Paris 6, Boîte Postal 99, 75252 Paris 05, France.

*To whom correspondence should be addressed. E-mail: forget@lmd.jussieu.fr

the youngest geological features on Mars (*4*). On Mars currently, the daily mean temperatures are much lower than 0°C, making it difficult for a significant amount of liquid water to survive at or near the surface. To explain the occurrence of the liquid flow which should have formed these gullies, Malin and Edgett (*1*) put forward a scenario involving groundwater seepage from a subsurface liquid water reservoir or aquifer located a few hundred meters or less below the surface. However, the process able to maintain such a shallow aquifer at temperatures above the freezing point of water remains unclear. Geothermal heating has been invoked to melt the martian ground ice (*5*–*7*), but there is no clear association between the location of debris flows and the general distribution of recent geothermal activity (*1*). Furthermore, gullies originating from the top of isolated peaks (*8*) and from the crests of large dark dunes (Fig. 1C) have recently been observed. In these cases, the involvement of a subsurface aquifer is unlikely.

Debris-flow landforms similar to the martian gullies are often observed on Earth. These debris flows consist of a mixture of unsorted rocky material with low water content that forms a muddy slurry which moves downslope (*9*). We observed and analyzed periglacial debris flows on the eastern cuesta of Jameson Land (East Greenland) (*10, 11*) where the mean annual temperature is –8°C. The permafrost is 80 to 220 m thick, and the active layer (part of the frozen ground thawing in summer) is about 1 m thick. Debris flows usually start from deep alcoves carved into the upper sandstone cornices (Fig. 1B). These debris flows exhibit single linear channels with lateral ridges (levées) and distal cones or fans like many of the martian gullies (Fig. 1A). Field observations indicate that the debris flows result from the thawing of snow and ground ice (*12*). This process is helped by the action of freeze-thaw cycles, which fracture the rocks and form debris (*11, 13*). During the summer, the debris becomes impregnated with liquid water that was produced by the melting of the seasonal snow cover, the interstitial ice within the active layer, and sometimes the underlying permafrost (*14*). Debris flows are usually initiated when the critical shear stress is reached after the increase of fluid pressure within the layer of weathered debris (*15, 16*). Nevertheless, debris flows with only 10% water by volume have been reported (*9*).

The analogy between gullies on Mars and debris flows in Greenland is striking. Both features exhibit the same length and the same morphology (Fig. 1). However, the process observed in Greenland cannot occur on Mars as we know it. It is a cold and dry planet where precipitation is negligible. Moreover, most of the observed martian gullies have been found on the southern plateau where, currently, the surface pressure is typically between 500 and 600 Pa, below the triple point of water at 610 Pa. However, higher pressures were possible when Mars's obliquity was higher, as recently as a few hundred thousand years ago (*17, 18*), because of the desorption of CO_2 from the high-latitude regolith and the sublimation of the permanent CO_2 ice polar cap (*19*). In such conditions, liquid water could probably flow over the length of the gullies, assuming water temperature at or slightly above 0°C (*20*). Spacecraft observations and climate models have shown that surface temperatures above 0°C are currently relatively common on Mars during summer afternoons (*21*). However, such conditions last for a few hours at most, and only the first few millimeters of the ground can be warmed above the melting point of water. This portion of the ground should be completely desiccated when temperatures increase enough to allow liquid water to be stable.

To melt water ice in the deeper subsurface, daily average temperatures above 0°C are necessary, so that the thermal wave can propagate to a significant portion of the ground. To investigate where such conditions could be or could have been achieved on Mars, we performed calculations of the surface and subsurface temperature on Mars for various latitudes, obliquities, surface slope angles, and orientations. For this purpose, we used a one-dimensional version of a global climate model (*22*). In this version, the diurnal and seasonal evolution of the surface and subsurface temperatures is governed by the balance between radiative and turbulent fluxes, thermal conduction in the soil, and CO_2 condensation and sublimation when necessary. This model has been extensively validated through comparisons with available spacecraft observations (*23*). For the present work, we added the capability to compute the ground temperature on a slope (*24*) and performed all of our calculations assuming surface, atmosphere, and orbit characteristics typical of Mars today (*25*). These calculations reveal that the only places on Mars where the daily mean temperature has been above the melting point of water during the past obliquity cycles are the mid- and high latitudes above 30°, especially on poleward-facing slopes around the summer solstice (Fig. 2). The corresponding thermal wave could have melted the ice down to 10 to 50 cm, depending on the conductivity assumed for the subsurface (Fig. 3). The fact that poleward-facing slopes receive more sunlight and get warmer at high obliquity in the sum-

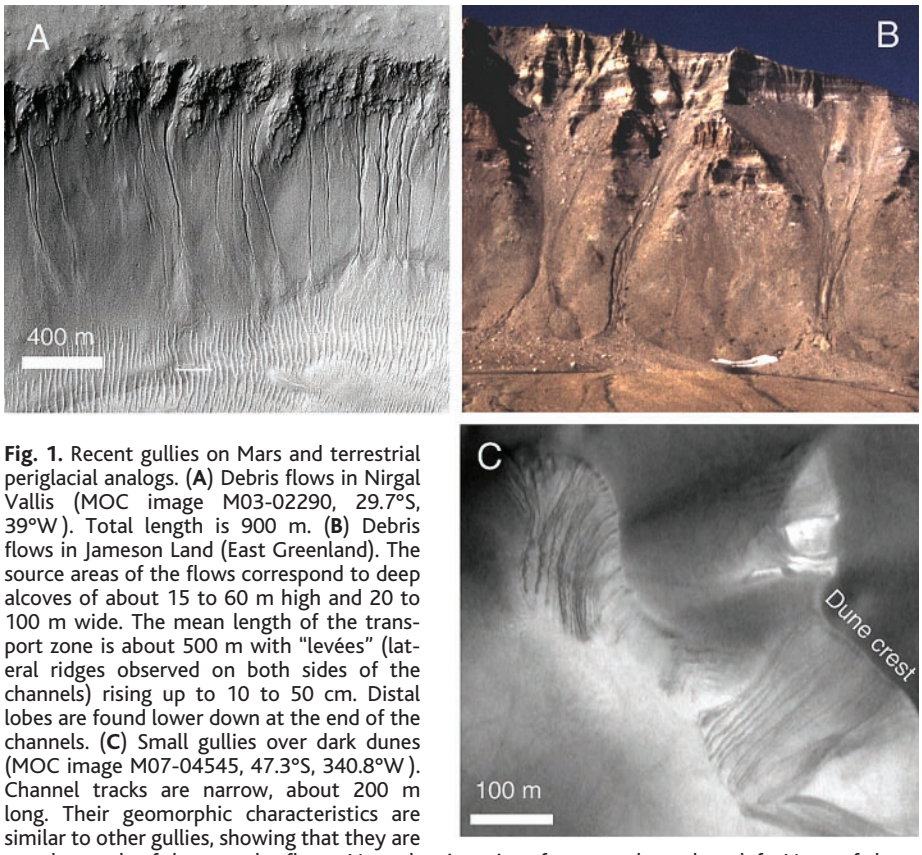

Fig. 1. Recent gullies on Mars and terrestrial periglacial analogs. (**A**) Debris flows in Nirgal Vallis (MOC image M03-02290, 29.7°S, 39°W). Total length is 900 m. (**B**) Debris flows in Jameson Land (East Greenland). The source areas of the flows correspond to deep alcoves of about 15 to 60 m high and 20 to 100 m wide. The mean length of the transport zone is about 500 m with "levées" (lateral ridges observed on both sides of the channels) rising up to 10 to 50 cm. Distal lobes are found lower down at the end of the channels. (**C**) Small gullies over dark dunes (MOC image M07-04545, 47.3°S, 340.8°W). Channel tracks are narrow, about 200 m long. Their geomorphic characteristics are similar to other gullies, showing that they are not the result of dry granular flows. Note the sinuosity of narrow channels at left. None of these gullies on dunes are observed on equatorward-facing slopes.

mer is due to the pole being tilted toward the sun. This preferential orientation and the latitudinal distribution of the warmest near-surface temperature coincide with the location of the observed martian gullies, suggesting a link between near-surface warming and debris flows. To further test this hypothesis, we performed a more detailed comparison between model and observations. We determined the orientation of 213 gullies identified in the MOC images data archive in the southern hemisphere [Web fig. 1 (*26*)]. At latitudes from 28°S to 40°S, almost all gullies face south (including southeast and southwest) with only 4% facing east. This agrees with the model, which predicts surface melting only for south-facing slopes at these latitudes (Fig. 2A). From 40°S to 60°S, 33% of the gullies are oriented east or west, but the south direction remains strongly dominant (55%) compared to the north (11%). In polar regions (60°S to 80°S), 35% of the gullies face north and 58% face south. This agrees with the model, which predicts that daily average temperatures above 0°C are also possible on both south- and north-facing slopes poleward of 60° (Fig. 2B).

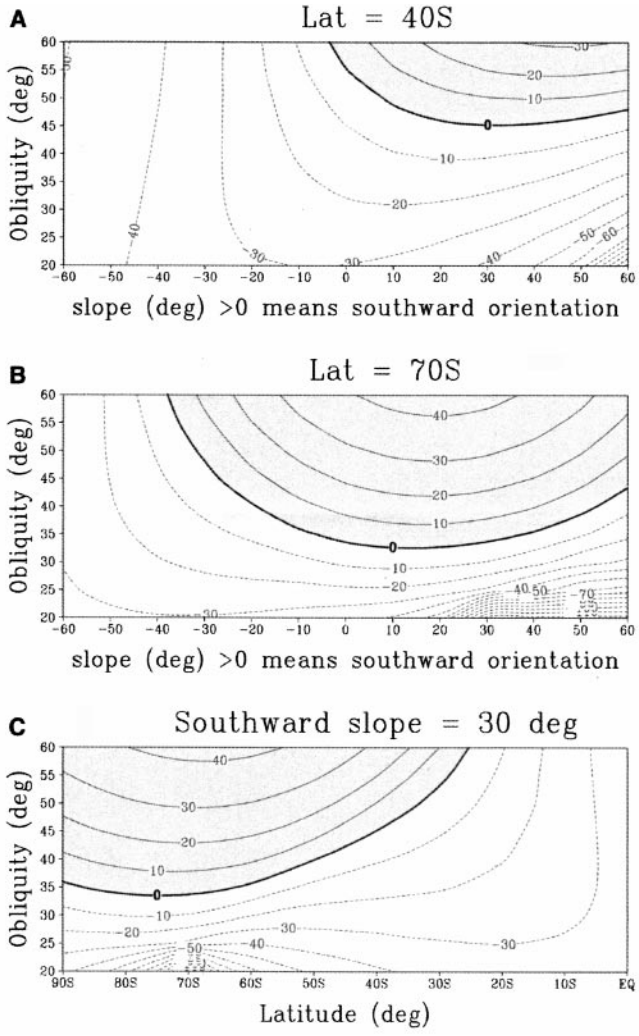

Fig. 2. Maximum of the daily average temperature on Mars (**A**) at 40°S latitude as a function of obliquity and slope, (**B**) the same at 70°S latitude, and (**C**) on a 30° poleward-facing slope typical of the location of the martian gullies. The daily average temperature is usually close to the subsurface temperature at depth z_1 as defined in Fig. 3. Above-freezing temperatures are predicted for obliquities above 33° on poleward-facing slopes at mid- and high latitudes, exactly where the gullies are found on Mars.

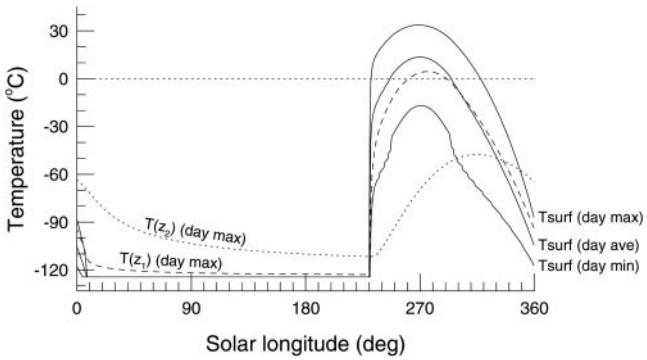

Fig. 3. Seasonal evolution of the surface and subsurface temperature on a 30° poleward-facing slope at 50°S latitude on Mars with an obliquity of 45°, as has often occurred on Mars, the last time possibly being about 6 million years ago (*17*, *18*). Solar longitude is 0° at the northern vernal equinox, and 270° at southern summer solstice. Solid lines show the daily average, minimum, and maximum surface temperatures. Dashed and dotted lines show the evolution of the daily maximum of the subsurface temperature at depth "z_1" and "z_2" corresponding to the skin depth for periods of 4.67 and 32.4 martian days (sols), respectively. z_1 and z_2 thus depend on the properties of the ground. For instance, z_1 = 0.36 m and z_2 = 3 m in an ice-rich permafrost (conductivity λ = 2 W m^{-1} K^{-1}, thermal inertia I = 1414 J m^{-2} s$^{-1/2}$ K^{-1}, volume heat capacity C = 10^6 J m^{-3} K^{-1}), and z_1 = 0.1 m and z_2 = 0.8 m in a typical dry and porous martian surface layer (λ = 0.068 W m^{-1} K^{-1}, I = 260 J m^{-2} s$^{-1/2}$ K^{-1}, C = 10^6 J m^{-3} K^{-1}).

Water is expected to have been present in the near subsurface at the location of the gullies when the obliquity was high. Mars at high obliquity was a relatively water-rich world because of the increased summertime sublimation of the water residual cap (*27*–*29*). Three-dimensional general circulation model simulations of the water cycle at 45° obliquity predict a column of atmospheric water vapor larger than 1000 precipitable micrometers around summer solstice in the southern hemisphere, compared to about 20 precipitable micrometers today (*28*). In such conditions, Mellon and Jakosky (*29*) have shown that, on average, water ice is expected to accumulate in the top few meters of the regolith up to 5 to 15 cm below a flat surface for obliquities larger than about 30°. On a poleward-facing slope at mid- and high latitude, water ice should get even closer to the surface because the annual mean temperature is lower than that on a flat surface. Water ice accumulates during most of the year when the ground temperature is low. Water can come from the atmosphere, the seasonal caps, and from the ice-rich subsurface because it is then warmer than the surface (Fig. 3B) (*29*). Around the summer solstice, the near-surface ground which is progressively warmed toward 0°C may tend to lose the water trapped in its pores through the diffusion of H_2O molecules into the atmosphere. However, on poleward-facing slopes, the seasonal CO_2 ice layer accumulated during fall and winter maintains the surface at the low CO_2 frost-point temperature until late spring (Fig. 3). The solar flux is then already strong. The disappearance of CO_2 ice allows a sudden warming of the surface and of the near subsurface which reach 0°C in a few days (Fig. 3). If any water is then present in the soil, it may not have time to completely diffuse out of the ground, especially because the atmospheric water content is then near its peak (diffusion primarily depends on the ground-atmosphere water density gradient).

Mars at high obliquity was a planet different than that of today, on which periglacial

phenomena, such as debris flows formed by melting of near-surface ground ice, were possible. In practice, such debris flows may have only occurred in some favored areas, because a relatively large amount of water is required in combination with the presence of cohesionless material (in East Greenland, debris flows are not generalized but only occur where large amount of debris is produced). Nevertheless, the possible presence of limited amounts of liquid water in the near surface at mid- and high latitudes predicted by our model have interesting consequences. It could induce freeze-thaw cycle erosion on Mars, and explain the polygons and patterned ground observed on MOC images (*8*) around 60° latitude, which look similar to terrestrial polygons related to the seasonal thawing of ground.

References and Notes

1. M. C. Malin, K. E. Edgett, *Science* **288**, 2330 (2000).
2. D. S. Musselwhite, T. D. Swindle, J. I. Lunine, *Geophys. Res. Lett.* **28**, 1283 (2001).
3. L. P. Knauth, S. Klonowski, D. Burt, *Science* **290**, 711 (2000).
4. However, we did find some alcoves and gullies covered by dust and a few impacts that could correspond to older debris flows. See, for example, MOC images M00-00530 and M03-01969.
5. W. K. Hartman, *Space Sci. Rev.* **96**, 405 (2001).
6. M. T. Mellon, R. J. Phillips, *Lunar Planet. Sci. Conf.* **32**, abstract no. 1182 (2001).
7. E. J. Gaidos, *Icarus* **153**, 218 (2001).
8. V. R. Baker, *Nature* **412**, 228 (2001).
9. A. M. Johnson, J. R. Rodine, in *Slope Instability*, D. Brundsen, D. B. Prior, Eds. (Wiley, New York, 1984).
10. Debris flows in East Greenland were observed by two of us during two field trips in July 1987 and August 1989. Jameson Land (70°N) is located north of the Scoresby Sund fjord and comprises wide plateaus 600 to 1000 m high mainly composed of clastic sediments (Permian to Lower Cretaceous age).
11. J. P. Peulvast, *Geogr. Ann. Ser. A* **70**, 351 (1988).
12. In the dry periglacial environment of Jameson land, direct runoff from rain is not thought to be the main process creating debris flows, although summer rains can contribute to the erosion of the plateau through shallow hortonian gullying on bare slopes. The mean annual precipitation is estimated to be only about 200 to 250 mm, mainly as snowfalls. Also, water springs were not observed where debris flows form.
13. J. L. Innes, *Phys. Geogr.* **7**, 469 (1983).
14. S. A. Harris, C. A. Gustafson, *Z. Geomorphol. N.F* **37**, 41 (1993).
15. P. A. Allen, *Earth Surface Processes* (Blackwell Science, Oxford, UK, 1997).
16. Navier-Coulomb law gives $\tau = C + (\sigma - P)\tan\phi$, where τ is the critical shear stress at failure, C the cohesion, σ the normal stress, P the pore fluid pressure, and ϕ the coefficient of internal friction. As the fluid pressure increases, the shear stress decreases and failure may occur. This process is efficient on steep slopes because the dry material is already near the critical shear stress before incorporation of water. Consequently, debris flows usually start at the most elevated point of debris aprons. This may explain the observation that some martian debris flows seem to start at the same level underneath scarps (Fig. 1).
17. J. Touma, J. Wisdom, *Science* **259**, 1294 (1993).
18. J. Laskar, *Celestial Mech.* **64**, 115 (1999).
19. H. H. Kieffer, A. P. Zent, in *Mars*, H. H. Kieffer, B. M. Jakosky, C. W. Snyder, M. S. Matthews, Eds. (Univ. of Arizona Press, Tuscon, AZ, 1992).
20. M. H. Carr, *Icarus* **56**, 47 (1983).
21. T. Z. Martin, A. R. Peterfreund, E. D. Miner, H. H. Kieffer, G. E. Hunt, *J. Geophys. Res.* **84**, 2830 (1979).
22. F. Forget *et al.*, *J. Geophys. Res.* **104**, 24155 (1999).
23. S. R. Lewis *et al.*, *J. Geophys. Res.* **104**, 24177 (1999).
24. To calculate the surface energy balance on a slope, the incident direct solar flux was modified to account for the actual sun incident angle on the slope. The solar flux scattered by the airborne dust was also modified, assuming that 50% of the scattered flux is coming from the direction of the sun and that the other 50% is more isotropic and thus not affected by the orientation of the slope. This assumption is supported by three-dimensional Monte Carlo simulations performed separately, which showed that, for opacity below unity, about 50% of the scattered light typically originates from less than a 15% portion of the sky centered on the sun.
25. The calculation shown here corresponds to the last year of 3.5-year simulations performed with a 30-min time step. We assumed a surface pressure of 700 Pa and a visible dust optical depth $\tau = 0.2$. Surface emissivity, thermal inertia, ground albedo, and CO_2 ice albedo were set to 0.95, 260 SI, 0.2, and 0.5, respectively. In practice, our results were found to be quite insensitive to the variations of these parameters, giving us some confidence in our ability to apply our conclusions to other epochs with different obliquities. The maximum diurnal averaged temperature significantly changes only in the case of large dust opacity (–6 K for $\tau = 1$, –18 K for $\tau = 5$).
26. Web fig. 1 is available at Science *Online* at www.sciencemag.org/cgi/content/full/1066698/DC1.
27. O. B. Toon *et al.*, *Icarus* **44**, 552 (1980).
28. M. I. Richardson, R. J. Wilson, *Bull. Am. Astron. Soc.* **32**, 1092 (2001).
29. M. T. Mellon, B. M. Jakosky, *J. Geophys. Res.* **100**, 11781 (1995).

30. We thank D. Mercier, P. Coussot, and R. M. Haberle for helpful discussions. We acknowledge the use of MOC images processed by Malin Space Science Systems. The Mars climate model has been developed in collaboration with the University of Oxford with the support of CNRS, the European Space Agency [TRP contract 11369/95/NL/JG(SC)], and the Centre National d'Etudes Spatiales. Supported by the Programme National de Planétologie, Institut National des Sciences de l'Univers, CNRS, France.

1 October 2001; accepted 16 November 2001
Published online 29 November 2001;
10.1126/science.1066698
Include this information when citing this paper.

Quantifying Uncertainties in Climate System Properties with the Use of Recent Climate Observations

Chris E. Forest,[1]* Peter H. Stone,[1] Andrei P. Sokolov,[1] Myles R. Allen,[2] Mort D. Webster[1]†

We derive joint probability density distributions for three key uncertain properties of the climate system, using an optimal fingerprinting approach to compare simulations of an intermediate complexity climate model with three distinct diagnostics of recent climate observations. On the basis of the marginal probability distributions, the 5 to 95% confidence intervals are 1.4 to 7.7 kelvin for climate sensitivity and −0.30 to −0.95 watt per square meter for the net aerosol forcing. The oceanic heat uptake is not well constrained, but ocean temperature observations do help to constrain climate sensitivity. The uncertainty in the net aerosol forcing is much smaller than the uncertainty range for the indirect aerosol forcing alone given in the Intergovernmental Panel on Climate Change Third Assessment Report.

Estimation of the uncertainty in long-term climate projections requires estimates of the probability density functions (pdfs) of key properties of the climate system. Attempts thus far (*1*, *2*) have used pdfs based on expert judgment to analyze such uncertainty. For near-term climate change, recent studies (*3*) have applied the uncertainty estimates derived from the climate change detection algorithm for particular models to climate projections based on these models. A key assumption in this approach is that both forcing and response do not change qualitatively between observed and forecast periods. Hence, it is not applicable to modeled climate change under scenarios that differ substantially from the recent past (e.g., stabilization cases or severe changes in sulfur emissions). Given the political priority to establish what constitutes a "safe" stabilization level for greenhouse gases, an objective means of quantifying uncertainty in the long-term response, despite uncertainty in other forcings, is clearly desirable.

These problems can be addressed in large part by determining both the range of climate system properties and the range of forcings that produce simulations consistent with

[1]Joint Program on the Science Policy of Global Change, Massachusetts Institute of Technology, Cambridge, MA 02139, USA. [2]Department of Physics, Oxford University, Oxford, OX1 3PU UK.

*To whom correspondence should be addressed. E-mail: ceforest@mit.edu

†Present address: Department of Public Policy, University of North Carolina, Chapel Hill, NC 27599, USA.